THE ASTROPHYSICAL JOURNAL, 244: 723–735, 1981 March 15

THE TRIPLE QUASAR Q1115+080A, B, C: A QUINTUPLE GRAVITATIONAL LENS IMAGE?

PETER YOUNG, ROBERT S. DEVERILL, JAMES E. GUNN, AND JAMES A. WESTPHAL
Palomar Observatory, California Institute of Technology

AND

JEROME KRISTIAN
Mount Wilson and Las Campanas Observatories, Carnegie Institution of Washington
Received 1980 July 28; accepted 1980 October 1

ABSTRACT

Spectroscopy and direct imaging of Q1115+080A, B, C with a CCD camera supports the hypothesis that they are gravitational images of a single object. Spectroscopy of the C III] λ1909 emission line shows all the images to have identical spectra and redshifts (to within 100 km s^{-1}), except that B is slightly redder. The position and brightness of the three images has been accurately measured; the images A, B, and C are magnitudes 16.30, 18.64, and 18.17, respectively, in the *r* band. B is 1".77 from A in position angle 266°, and C is 2".28 away at position angle 322°. A and C have the same color, but B is redder by 0.23 mag in $(g-r)$. There is no trace of a lens galaxy, which must have a surface brightness of less than 29 mag $arcsec^{-2}$ at a distance of 5"–8" from Q1115+080. Three bright galaxies lie near Q1115+080, apparently forming a small group. Gravitational lens imaging by a massive spiral galaxy is explored, and we find a quintuple image model resembling Q1115+080A, B, C. In this model, Q1115+080A is a highly magnified close pair of images oriented in position angle 23°. An elongation of Q1115+080A at this angle is seen in the CCD pictures.

Subject headings: galaxies: clusters of — gravitation — quasars

I. INTRODUCTION

The quasar Q1115+080 was discovered to be a close triplet of images by Weymann *et al.* (1980). The bright object Q1115+080A is 16 mag, and there is a pair of objects (B and C) of 18 mag only 2" from A. Weymann *et al.* obtained spectra of Q1115+080A, B, C which show that all three objects have identical spectra with a redshift $z_s = 1.722$. This may be a second case of a gravitational lens. The first such case is Q0957+561A, B which is described in detail in Young *et al.* (1980, 1981; hereafter Papers I and II).

We have obtained both direct and spectroscopic CCD data on Q1115+080 in good seeing. We confirm the spectroscopic equality of the images, and we present accurate magnitudes and positions for Q1115+080A, B, C. Because there are apparently three images, a strong case can be made for a gravitational lens effect even though the object responsible for the multiple imaging of Q1115+080 is not seen. As we pointed out in Paper I, a nonsingular mass distribution must produce an odd number of images, normally three. In the case of Q0957+561A, B only two images are visible, and the third image awaits discovery. In Q1115+080A, B, C three images are apparently visible. Theoretical modeling with imaging by a massive spiral galaxy demands that there be five images and that Q1115+080A be a highly magnified close double. Inspection of our CCD data shows an elongation of Q1115+080A in the predicted position angle of 23°. The fifth image is not seen in our data; the model predicts that it is quite faint.

II. SPECTROSCOPIC OBSERVATIONS

a) Instrumentation

All observations were made with the 200 inch (5.08m) Hale reflector equipped with the prime focus universal extragalactic instrument (PFUEI) as described in Gunn, Hoessel, and Westphal (1981) and Paper I. This device may be used as a camera or a spectrograph and images onto a 500×500 low-noise CCD. Both spectroscopic and photometric observations of Q1115+080 were made on five nights in 1980 June. A journal of observations is given in Table 1.

For spectroscopy, we used a 400 line mm^{-1} transmission grating blazed at 5000 Å. A slit of dimensions 1".5×150" and a dispersion of 440 Å mm^{-1} gave 6.5 Å per 15 μ pixel on the CCD and a spectral resolution of 25 Å.

The observations were made by setting the slit across two of the images, either A and B or A and C, as

TABLE 1

JOURNAL OF OBSERVATIONS

UT Start (1980 June)	Filter[a]	Exposure (s)	No. of Frames	Airmass	Seeing FWHM (arcsec)	Images Observed
13.20.....	*r*	100	1	1.57	1.37	...
14.19.....	*r*	2000	5	1.65	1.42	...
15.17.....	*r*	800	8	1.44	1.32	...
15.20.....	λλ4893–6856	2000	2	1.82	1.57	A, B
16.17.....	*r*	200	2	1.44	1.25	...
16.18.....	*i*	400	3	1.48	1.29	...
16.19.....	*g*	400	2	1.56	1.32	...
16.20.....	λλ4893–6856	2000	2	1.83	1.58	A, B
16.25.....	λλ4893–6856	2000	2	3.55	1.75	A, C
17.18.....	*i*	100	1	1.49	1.60	...
17.18.....	*g*	150	1	1.52	1.37	...
17.18.....	*r*	100	1	1.54	1.37	...
17.19.....	*i*	1000	10	1.66	1.80	...
17.21.....	λλ4893–6856	2000	2	1.95	1.60	A, C

[a] A wavelength range given here indicates a spectroscopic observation. Other observations are photometric in the *uvgri* system of Thuan and Gunn (1976) of Thuan and Gunn (1976).

shown in Table 1. This is in order that the scattered light from component A can be accurately subtracted from the faint image.

The spectral region λλ4893–6856 was observed. This includes the emission line of C III] λ1909 at 5196 Å. The Mg II λ2799 is at 7619 Å and is suppressed by the atmospheric A band. The only other strong emission line is C IV λ1549 at 4216 Å, which we did not observe because the CCD has a quantum efficiency of only 12% at that wavelength.

b) Reductions

The two-dimensional spectra of Q1115+080A and B were reduced in the following manner:

1. The sky signal was obtained using regions external to the spectra of Q1115+080. The sky was subtracted from the entire picture to leave only the spectra of Q1115+080.

2. Three one-dimensional spectra were extracted from the two-dimensional picture; they are denoted BS, A, and BF. If Q1115+080A is centered at spatial coordinate X_A then spectrum A is obtained by summing the signal from $(X_A-\delta)$ to $(X_A+\delta)$. We used a value $\delta=0''.84$. The signal from $(X_A+X_{AB}-\delta)$ to $(X_A+X_{AB}+\delta)$ was used for spectrum BF which contains Q1115+080B plus spillover from Q1115+080A. We used a value $X_{AB}=1''.8$. The spectrum BS was obtained from spatial positions $(X_A-X_{AB}-\delta)$ to $(X_A-X_{AB}+\delta)$, which gives the amount of signal from Q1115+080A contaminating spectrum BF (the spatial profile of the PFUEI is symmetric as was determined from exposures on bright stars).

3. The quotient BS/A was fitted with a polynomial:

$$\mathrm{BS}(\lambda)/\mathrm{A}(\lambda)+\varepsilon(\lambda)=\sum_{i=0}^{4} a_i\lambda^i=p(\lambda), \qquad (1a)$$

where $\varepsilon(\lambda)$ is the residual from the least-squares fit. The decontamination of spectrum BF to get a spectrum of B was done using:

$$\mathrm{B}(\lambda)=\mathrm{BF}(\lambda)-p(\lambda)\mathrm{A}(\lambda). \qquad (1b)$$

About 30% of the signal in BF was spillover from Q1115+080A. The spectra of Q1115+080A and C were reduced with $X_{AC}=2''.3$ and had a contamination level of 10% in the spectrum of C prior to its being cleaned.

c) The Spectra

First, we present in Figure 1 the sum of all four spectroscopic observations listed in Table 1. This includes four spectra of component A and two spectra each of B and C; however, the spectra of A dominate since it is by far the brightest image. We have declined to reduce the spectral data to a flux standard since the low altitude of Q1115+080 during the observations resulted in considerable differential refraction effects. Absolute fluxes, from the broad-band photometry, will be given in the next section.

The summed spectrum shows strong C III] λ1909 emission. Nestled in the blue wing of this line is a small emission bump which we measured to be at a rest wavelength of 1860±2 Å; it is probably the Al III λ1858 resonance doublet. Another clear emission bump appears at a rest wavelength of 2073±2 Å. This might be Si II λ2073 (multiplet 9) or Fe III λλ2061, 2068, 2078 (multiplet 48) or something else. Undulations in the spectrum appear at 2250–2400 Å (rest wavelengths) which may be due to a swath of Fe II emission from multiplets 2, 3, 4, and 5.

In Figure 2 we compare spectra of Q1115+080A, B from the observations listed in Table 1. The spectrum of A is shown along with the decontaminated spectrum

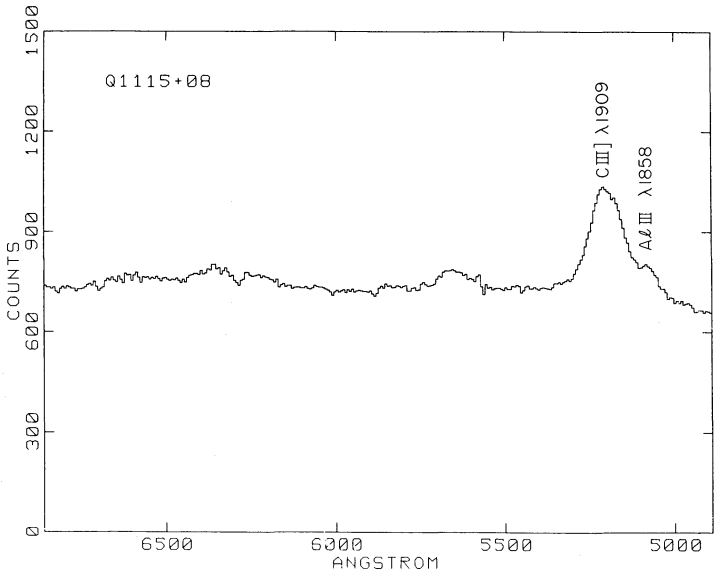

FIG. 1.—Summed spectra of Q1115+080A, B, C. Each bin is 6.5 Å and the spectral resolution is 25 Å. The redshift is $z_s = 1.7225$ with strong C III] λ1909 emission visible (C IV λ1549 is visible in the spectra of Weymann *et al.* 1980).

of B. The quotient B/A is also shown, as well as the quotient after being fitted with a straight line. The slight difference in continuum slope between A and B is probably real since differential refraction afflicts both images equally. Further, the effect shows up in the photometry, as we shall see in § III. The spectra of A and B are identical apart from some slow undulations left in the quotient. In Q0957+561 such undulations revealed the presence of the lens galaxy. Here it is not clear what is going on. As we shall see in § III*c*, the lens galaxy must be very faint and we may either be seeing very slight traces of it, or the undulations may be dust features from a dust cloud which reddens Q1115+080B.

In Figure 3 we show a similar tableau of spectra for Q1115+080A and C. For the position angle of A and C, differential refraction effects are much more severe than for A and B, since the atmospheric dispersion was orthogonal to the slit. Since we guided on the *g* (λ5000) position of the object, there is a drop in flux to the red. This explains why the continuum slope of Q1115+080A is very different in Figures 2 and 3. The error in the position angle of A and C reported by Weymann *et al.* (1980), to which we set the slit, causes the difference in the continuum slopes of A and C (photometry in § III shows A and C to be the same color).

d) C III] λ*1909 Emission*

The appearance of this emission line is similar in all three components, including the satellite emission line Al III λ1858 in the blue wing. We have measured the position and equivalent width of the emission line in all three components.

The redshift was obtained by solving

$$\sum_i (\lambda_i - \lambda_o) \exp\{-(\lambda_i - \lambda_o)^2 / 2\sigma^2\} A_i = 0, \quad (2)$$

where A_i is the data number in the ith channel of the spectrum of component A (for example), λ_i is the wavelength of this channel, λ_o is the position of line to be found, and σ is a fixed parameter. Prior to solving this equation, the spectra were normalized to have a continuum of unity everywhere (to remove problems associated with the different continuum slopes in the observations). For a symmetric line, equation (2) gives the centroid. If the line is not symmetric (as it is not because of the Al III λ1858 emission), then equation (2) gives a quantity other than the centroid. Since we are anxious to test the null hypothesis that the line profiles in Q1115+080A, B, C are identical, it does not matter what parameter is measured as long as the same thing is done to each spectrum. Equation (2) has the advantage of being the best measurement it is possible to make on a roughly Gaussian line (by "best" we mean minimum variances in λ_0). We measured λ_0 with σ set to 33 Å. This is somewhat smaller than the Gaussian dispersion of the emission line, but it lessens the effect of Al III λ1858 emission which is to pull the line position to the blue. The equivalent width measurements of the line were made in the spectra whose continua were normalized to unity, and they include both C III] λ1909 and Al III λ1858 emission.

The results are shown in Table 2. The line positions in all objects are the same at the 100 km s^{-1} level. The equivalent widths in Q1115+080A and C are identical. The line is weaker in Q1115+080B, but this is a margi-

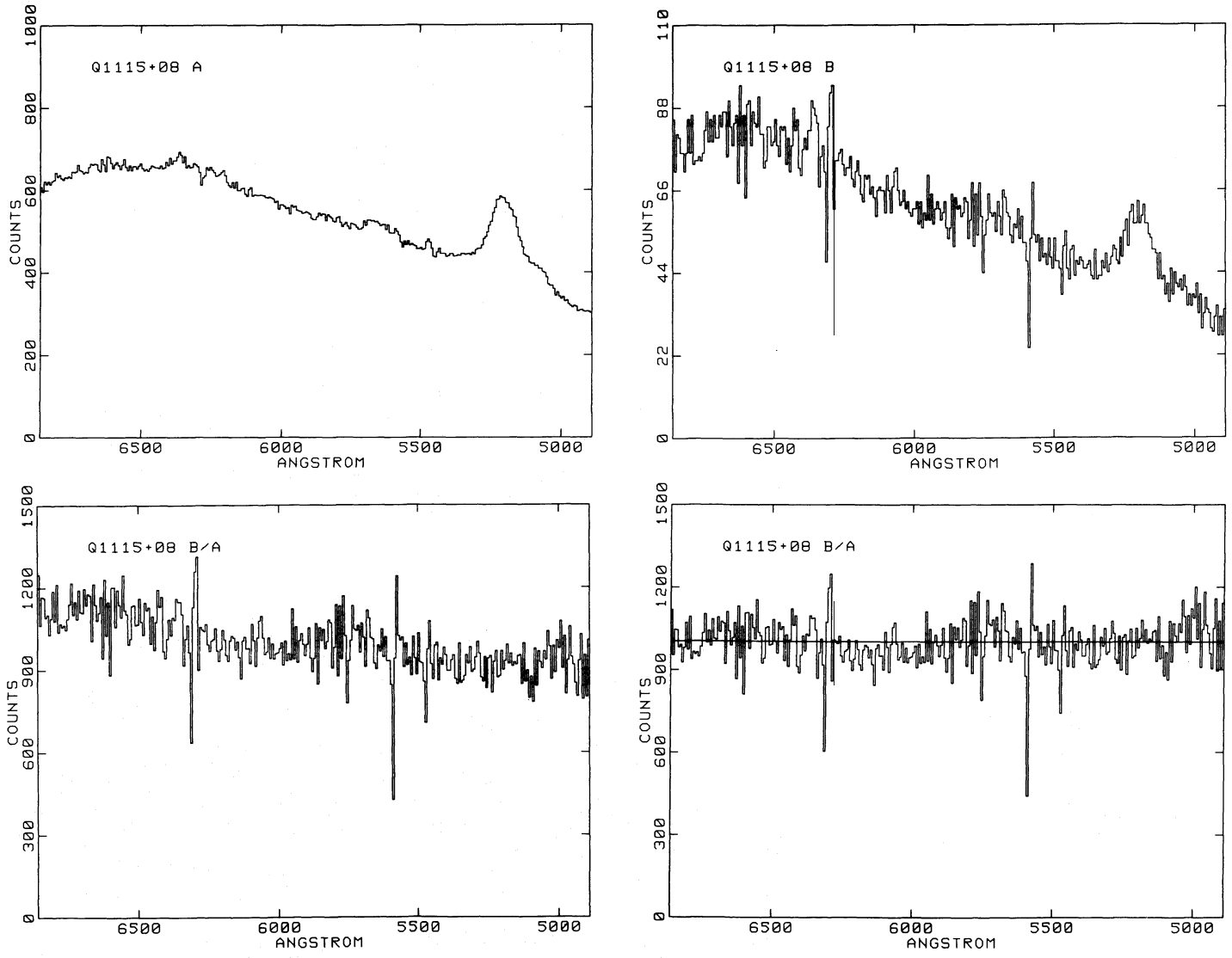

FIG. 2.—Comparison of spectra of Q1115+080A and B. The spectrum of A and the spectrum of B with scattered light from A removed are shown at the top. Differential refraction spilling light outside the 1".5 slit at airmasses 2–3 causes the spurious steep continuum slopes. Imperfect sky-line subtraction also results from the large airmasses. The quotient B/A is shown below, normalized to a mean of 1000 on the left and divided by a straight line on the right. The slight difference in continuum slope between B and A is probably real since the differential refraction affects both images equally (and the effect is shown in our photometry). The C III] λ1909 divides out well. The only features left in the quotient are possibly very slow undulations of the spectrum.

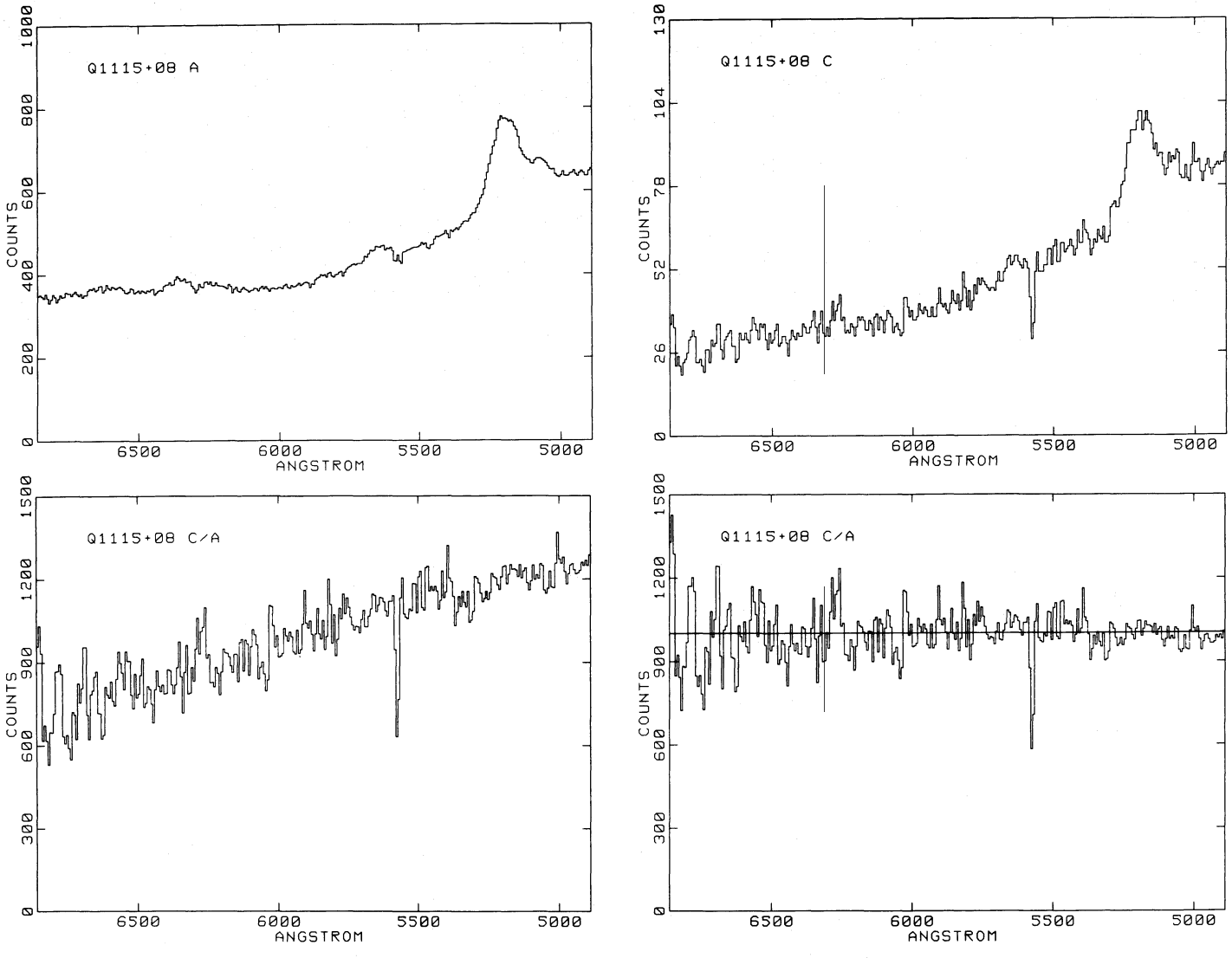

FIG. 3.—Comparison of spectra of Q1115+080A and C. This tableau is the same as is described in Fig. 2. The difference in continuum slope between Q1115+080 in Figs. 2 and 3 is caused by the different slit position angles and the consequent different differential refraction spillout. The difference in continuum slope between A and C is not real, but is caused by different differential refraction spillout (since we set the slit P.A. to the value given in Weymann *et al.* which is in error by 10°). C III] λ1909 divides out well, and there are no real features left in the quotient.

TABLE 2

C III] λ1909 EMISSION IN Q1115+080

Component	A	B	C
Wavelength (air) Å	5195.2±0.9	5196.2±2.2	5194.2±1.8
Redshift z_s	1.7225±0.0005	1.7230±0.0011	1.7220±0.0009
Velocity (km s^{-1}).....	0	58±137	−58±116
Equivalent Width (Å)[a] ...	65.9±1.4	59.9±3.3	65.2±2.9

[a]Includes Al III λ1858 emission in blue wing of C III] λ1909.

nal result at only the 1.8σ significance level. It should be noted that continuum variations in Q1115+080 could cause this since there are presumably some time delays among the images.

In summary, the spectra of all three objects are identical, except that Q1115+080B may have a slightly weaker emission line. The redshifts of the objects are the same to within 100 km s^{-1}. As in the case of Q0957+561A, B, the components are far more similar than one might expect for three quasars in a cluster. The fact that there are three identical objects must be considered good evidence for there being a gravitational lens effect.

III. PHOTOMETRIC OBSERVATIONS

a) Total Flux Measurements

The observations of 1980 June 17 in Table 1 were made under photometric conditions. The PFUEI camera was used in its direct mode to take broad-band pictures in the g(λ5000), r(λ6500), and i(λ8300) filters in the *uvgri* system (Thuan and Gunn 1976; Wade *et al.* 1979). Additional r, i observations on June 13 and 14 were made under photometric conditions and were used to check the primary photometry. From this, we estimate standard deviations of 0.01 mag in the flux measurements of A+B+C which are shown in Table 3. The total fluxes given are those within a circular aperture of 12".63 diameter centered 0".75 NW of the center of Q1115+080A.

b) Image Separations and Fluxes

Our best CCD pictures of Q1115+080 have a seeing FWHM of 1".2. Image C is clearly separated from A, and image B is visible as an extended tail on A to the west.

In Figure 4 we show contour plots of a 100-second r exposure on Q1115+080 in 1".2 seeing. We also show a nearby star to demonstrate the seeing plus instrumental profile. The distance of B from A is clearly much less than the distance of C from A.

We elected to solve for the image positions and fluxes by fitting a triple star to the three images. In order to cope with the discrete sampling of the star profile, we interpolated with the sampling theorem formula:

$$I(x,y)=\sum_{ij} S_{ij}\frac{\sin\pi(x-i)}{\pi(x-i)}\frac{\sin\pi(y-j)}{\pi(y-j)} \times\exp\left\{-\frac{(x-i)^2}{2\sigma^2}-\frac{(y-j)^2}{2\sigma^2}\right\}, \quad (3)$$

to define the star profile at all points (x, y) given its values S_{ij} at the integer points (i, j). The Gaussian filter was used to apodize the bandpass and quench ringing; the parameter σ was set to the Gaussian dispersion of the core of the star profile (typically 1.2 pixels). Image A is not quite a true stellar profile (see § IV*d*), so the star was convolved with a Gaussian before the fits were made. This broadened it to improve the fit to the A component while negligibly degrading the fit to components B and C.

We obtained a solution by a nonlinear least-squares fit of the star profile to the three images. Nine parameters (fluxes f_A, f_B, f_C; positions $x_A, y_A, x_B, y_B, x_C, y_C$) were allowed to vary. The best frames from June 16 in Table 1 were selected for the determination of the parameters. The results are shown in Table 4 for each of the seven frames with the various filters. The mean

TABLE 3

TOTAL FLUXES FROM Q1115+080

Filter	Wavelength (Å)	Photometric Magnitude	AB_ν Magnitude[a]
g	5000	16.04±0.01	16.06±0.01
r.....	6500	16.02±0.01	15.81±0.01
i.....	8300	15.90±0.01	15.60±0.01

[a]$AB_\nu = -2.5\log_{10} f_\nu - 48.60$.

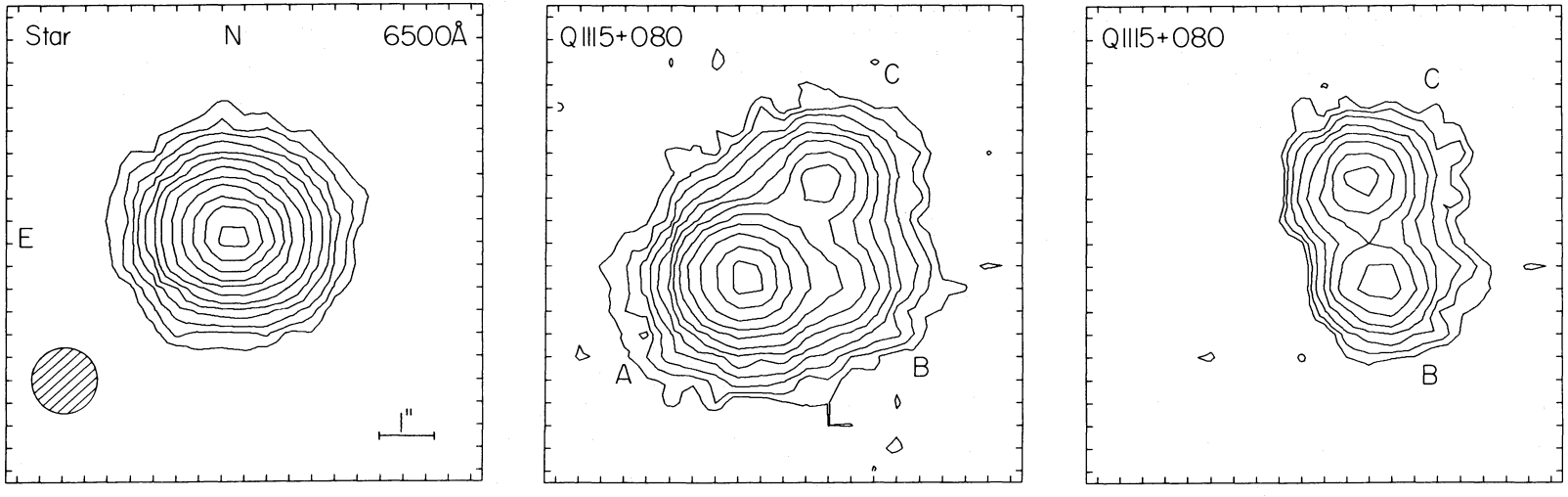

FIG. 4.—Contour plots of Q1115+080. The left-hand plot shows a field star with the seeing FWHM inset as a hatched circle. The central plot shows Q1115+080A, B, C and the right-hand plot has had Q1115+080A removed (by subtracting the field star after treatment to allow for the elongation of Q1115+080A in P.A. 30° (see § IV*d*)). The plots are from a 100-second *r* exposure in seeing 1".2. The tick marks on the plots each correspond to 1 pixel of 0".422. Contours are at intervals of 0.45 mag arcsec^{-2} in surface brightness above the sky. North is up and east to the left.

TABLE 4

Q1115+080B, C Positions and Fluxes Relative to A[a]

Filter	Seeing FWHM (arcsec)	f_B/f_A	$x_B - x_A$[b]	$y_B - y_A$[b]	f_C/f_A	$x_C - x_A$	$y_C - y_A$
r	1.25	0.114	−1.739	−0.118	0.176	−1.435	+1.781
r	1.26	0.124	−1.772	−0.093	0.181	−1.439	+1.810
i.....	1.30	0.112	−1.798	−0.093	0.190	−1.317	+1.853
i.....	1.25	0.118	−1.646	−0.063	0.177	−1.325	+1.819
i.....	1.34	0.145	−1.709	−0.122	0.203	−1.414	+1.772
g	1.46	0.087	−1.933	−0.216	0.183	−1.363	+1.794
g	1.19	0.101	−1.777	−0.215	0.164	−1.447	+1.798
Mean		0.114	−1.768	−0.131	0.182	−1.393	+1.802
$\sigma/n^{1/2}$		±0.006	±0.034	±0.021	±0.005	±0.021	±0.008

[a] From the seven frames taken on June 16.

[b] The coordinates have x pointing east and y pointing north. The units are seconds of arc.

positions determined from this subset of the data are taken as the true positions of the components. The purpose of this is to measure more accurate colors for the images by fixing the offsets from Q1115+080A. We assume, therefore, that the positions of the images are the same in the g, r, and i bands. This may not be true if the (presumed) lens galaxy contaminates one of the images, but we would then hope to see that image somewhat redder than the others. In Table 4 there is no dramatic difference in the fluxes or positions of the images in the different bands, although image B is slightly fainter in g. There are, however, strong correlations between some of the parameters (f_B and $x_B - x_A$, for example).

Our procedure of fixing the relative positions in order to determine the colors should give better results than those in Table 4, because the effects of correlations between parameters in the fit are reduced. The results of the fixed position calculations are shown in Table 5. The mean values do not differ much from those in Table 4. There is, however, a significant (4σ) tendency for image B to be fainter in g than r or i. This could quite easily be a result of a slight reddening of image B relative to A and C (the effect was also seen in the spectra in § II*c* despite the differential refraction problems).

The final set of parameters we have adopted is in Table 6. If the "reddening" of Q1115+080B is due to an intervening dust cloud, then f_B/f_A will be greater than the value given in Table 6. The size of the correction will depend on the redshift of the absorbing dust (e.g., if $z_d = 1.25$ the g(5000 Å) band will be subject to the λ2200 dust absorption feature). Alternatively, the lens galaxy itself, if it is near one of the images, may cause a slight reddening of that image, as was the case in Q0957+561.

In any case, the fact that the three images all have nearly the same, quite blue, colors is further evidence in favor of the gravitational lens hypothesis.

c) Limits on the Brightness of a Lens Galaxy

The lens galaxy (if it is a galaxy) might be detected by its outer regions being visible in the wings of the radial profile of Q1115+080. In order to look for this,

TABLE 5

Q1115+080B, C: Fluxes Relative to A[a]

Filter	Seeing FWHM (arcsec)	f_B/f_A	f_C/f_A
r	1.25	0.109	0.175
r	1.26	0.121	0.181
Mean r		0.115±0.006	0.178±0.003
i.....	1.30	0.108	0.185
i.....	1.25	0.106	0.176
i.....	1.34	0.140	0.202
Mean i		0.118±0.011	0.187±0.007
g	1.46	0.086	0.180
g	1.19	0.099	0.162
Mean g		0.093±0.007	0.171±0.009
Mean.....		0.110±0.006	0.180±0.004

[a] Using fixed positions from Table 4.

TABLE 6

Q1115+080A, B, C ADOPTED PARAMETERS

Image	A	B	C
g	16.29±0.02	18.87±0.06	18.21±0.05
r	16.30±0.02	18.64±0.05	18.17±0.02
i	16.19±0.02	18.51±0.09	18.01±0.04
$g-r$	−0.01±0.02	+0.23±0.07	+0.04±0.06
$r-i$	+0.11±0.02	+0.13±0.11	+0.16±0.05
f/f_A	1	0.110±0.006	0.180±0.004
$x-x_A$	0	−1″.768±0″.034	−1″.393±0″.021
$y-y_A$	0	−0″.131±0″.021	+1″.802±0″.008
Distance from A	0	1″.773±0″.034	2″.278±0″.015
P.A. from A	0	265°.8±0°.7	322°.3±0°.4

we measured three radial profiles on the sum of the r frames taken on June 14. These profiles were of: (1) Q1115+080A,B,C,; (2) a bright field star. In order to exactly mimic the Q1115+080 image, we formed a data frame:

$$D^*(x,y)=(f_A/f_S)D(x,y) + (f_B/f_S)D(x-x_B+x_A, y-y_B+y_A) + (f_C/f_S)D(x-x_C+x_A, y-y_C+y_A), \quad (4)$$

with $D(x,y)$ being the original data, and f_S the flux from the field star (the other symbols are as before); and (3) galaxy G1 (identified in § IIId).

In Figure 5 we show the difference between the radial profile of Q1115+080 and the "triple star" as defined by equation (4). Also shown is the radial profile of G1. In this plot, one "data number" corresponds to a surface brightness of 30.0 mag arcsec^{-2} in the r band. Except for a small rise inside 5″ (which is too precipitous to be a galaxy and is probably due to slight systematic differences between the instrumental profiles at the positions of the star and quasar), there is no trace of a galaxy. By comparison with G1, we could see a galaxy some 10 times fainter than G1, assuming it to have the same radial profile. Since we have measured the magnitude of G1 to be 18.96 in the r band (see § IIId), we would expect to be able to see a galaxy of 21.5 mag. Less stringent limits would apply to a more compact galaxy. The mean surface brightness of a lens galaxy, at radii from 5″ to 8″ from the center of Q1115+080, does not exceed 29.0 mag arcsec^{-2} in the r band. A brightest cluster elliptical galaxy would have to lie at $z_d > 0.8$ in order to be invisible to the present limit of 21.5 mag. We would expect to see a cluster associated with such a galaxy if it lies at a redshift of less than 1. As we shall see in § IV, it is not likely that a brightest cluster galaxy is responsible for the imaging because of the triangular geometry.

We finally note that the "reddening" of Q1115+080B noted in § IIIc is probably not due to the lens galaxy, unless that galaxy is unusually compact. A galaxy of 20 mag and $(g-r)=1$ would be needed to redden image B sufficiently; this would be visible easily in our radial profiles.

d) The Field around Q1115+080

In Figure 6 (Plate 8) we show a 2000-second CCD exposure in the r band (this being the summed data of June 14) stretched to display faint objects surrounding Q1115+080. The field, apart from Q1115+080, seems quite typical of "blank sky" as judged by the Palomar Ultra-Deep Survey (where we take deep exposures to do source counts). There is no cluster of galaxies as there was for Q0957+561.

Object S (as defined in Weymann *et al.* 1980) is a red star. There are three galaxies quite near to Q1115+080, which we have denoted G1, G2, and G3, and there is a bright barred-spiral foreground galaxy G0 some distance from the quasar. G1, G2, and G3 are brighter than the average galaxy in the frame and may form a

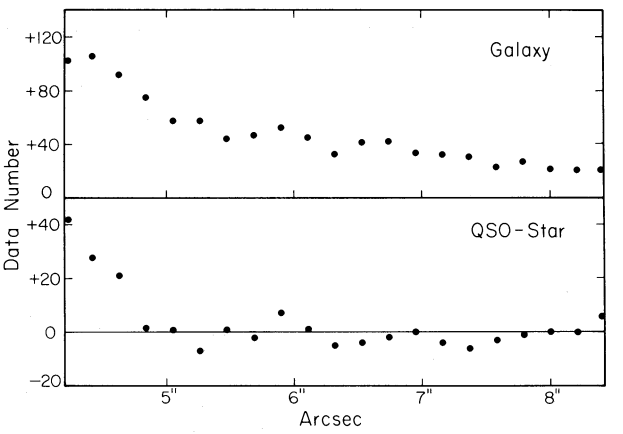

FIG. 5.—Radial profiles of galaxy G1 (top) and the difference between Q1115+080 and a suitably treated field star (bottom). One "data number" corresponds to 30.0 mag arcsec^{-2} in the r band.

small group. Galaxy G1 is the one used for the radial profiles in § III*c*.

Table 7 gives the *r* magnitudes and positions of galaxies G1, G2, and G3, and star S. For the galaxies, we give *total* magnitudes, as in Paper II. Redshifts for these galaxies would be interesting. If they are distant (and thus presumably massive), they could have a significant effect on the gravitational modeling.

IV. GRAVITATIONAL LENS MODELS

a) Possible Mass Configurations

An elliptical galaxy model of the type discussed in Papers I and II produces three images roughly in a line. Even if the galaxy has projected isophotes with an ellipticity $\varepsilon = 1 - b/a = 0.5$, the skew in the image line is quite modest. These models (together with the effects of the galaxy cluster) explained Q0957+561 quite well.

The triangular configuration of Q1115+080A, B, C is not explained by such models; the mass distribution needs to be more asymmetric than an E5 galaxy. Among some of the more or less plausible ideas that come to mind are:

1. Two or more galaxies act in combination.
2. The lens galaxy may be a massive spiral with both disk and halo components.
3. There may be five images; one of the observed images may be a close double with resultant high magnification near the "singular configuration." The fifth image would then have to be faint.
4. Galaxies G1, G2, and G3 could be distant and sufficiently massive to perturb the modeling action. Their main effect would be to shift the true position of the quasar and to change the time delays, as in our models of Q0957+561 (Paper II).
5. Image B is reddened. The accompanying extinction, if the reddening is due to a dust cloud, may mean B is, in reality, much brighter than observed.
6. There may be other images that cannot be seen because of strong absorption.

There are entirely too few parameters known to make a definitive solution of Q1115+080A, B, C. We feel that single galaxy models have a higher probability of occurring than multiple galaxy models, and that we should use a giant spiral galaxy mass distribution. Extinction will be assumed zero, unlikely though that is if the galaxy is a spiral (although if it is an S0 galaxy that will be a good assumption). Lastly, we shall place it arbitrarily at a redshift $z_d = 0.8$. If it is much smaller than this, the lens galaxy may be visible; if it is much larger, its mass density becomes implausibly large.

b) Imaging by a Massive Spiral Galaxy

The gravitational lens computer program with the formalism described in Paper II was used. In the notation of that paper, we use a surface mass distribution

$$\sigma_*(b_*) = 2\pi\{1 + b_*^2\}^{-X/2}, \qquad (5)$$

rather than the King model approximation given in Paper II. We used a slightly flattened mass distribution to represent the bulge component of the galaxy and a second, highly flattened mass distribution to model the disk component.

The free parameters were set as follows:

1. Bulge axis ratio $\cos\beta_B = 0.7$.
2. Bulge "velocity dispersion" $\sigma_v^B = 325$ km s^{-1}.
3. Bulge structural length $a_B = 2$ kpc.
4. Disk axis ratio $\cos\beta_D = 0.1$.
5. Disk velocity dispersion $\sigma_v^D = 735$ km s^{-1}.
6. Disk structural length $a_D = 3$ kpc.
7. Cosmological parameters $H_o = 60$ km s^{-1} Mpc^{-1}; $q_o = 0$.
8. Redshift of galaxy $z_d = 0.8$.
9. $X = 3/2$.

For observers who may become alarmed at the large velocity dispersions, we remind them that the values quoted here simply define the *mass density* and do not represent (even approximately) values that might be observed. In particular, the surface mass density of the disk is very high because it is so flattened, so the "velocity dispersion" is very high.

Our model has rather more mass in the bulge than the disk (ratio 1.36 to 1) in projected ellipses with the same major axis. It would represent a spiral inclined at 85° to the line of sight if the true disk axis ratio were 0.05. We set $X = 3/2$ to give a rotation curve declining as $r^{-1/4}$. The circular velocity is about 350 km s^{-1} at a radius of 10 kpc. This is a very massive spiral galaxy; it

TABLE 7

OBJECTS CLOSE TO Q1115+080

Object	*r*-Magnitude	$x - x_A$	$y - y_A$	r_e^a	σ_g^a
S.....	19.26±0.03	+ 5″.42±0″.02	−21″.82±0″.01	...	...
G1.....	18.96±0.05	−21″.53±0″.02	−10″.53±0″.01	3.46	0.05
G2.....	20.04±0.05	−12″.89±0″.02	− 0″.32±0″.02	3.33	0.67
G3.....	20.53±0.05	−15″.18±0″.03	−11″.68±0″.03	3.06	0.27

[a] The parameters r_e, σ_g give profile information for the galaxies, as described in Paper II.

can be made less massive by decreasing the redshift; there is then the danger of it becoming visible. The characteristic velocities required to yield images 2″ apart are ~250 km s^{-1}, indicating that the lens galaxy must be dense or massive; such a galaxy at $z_d = 0.5$ would be visible unless unusually compact (e.g., a high-density dwarf).

Until it is determined whether or not G1, G2, and G3 can affect the gravitational imaging, they will be neglected.

c) *Image Solutions*

Our intention is not to rigourously fit the data on Q1115+080 because of the various uncertainties discussed above. Rather, we wish to gain some insight into the sort of image pattern that results from a massive spiral galaxy as we have modeled it. We ran some image solutions for other spiral galaxy models, and they were qualitatively similar to the ones to be given here.

Some typical solutions are shown in Figure 7. We have not shown any single image solutions, only triplets and quintuplets. The most common solutions involve a "crooked line" of three images with two bright and one faint. Three examples of this are in Figure 7, and they bear no resemblance to Q1115+080. When the quasar is closer to the galaxy center, five images appear and the usual arrangement is a "crooked cross" with four bright images and the fifth one faint. Two examples of crooked crosses are shown in Figure 7. One is a normal crooked cross and bears no resemblance to Q1115+080. The other is a very crooked cross where two of the images are on the verge of merging and disappearing (and become greatly amplified; the closer to degeneracy the greater the amplification). This set of images resembles Q1115+080; the two close images would correspond to the A image, a negative parity image corresponds to B, and the positive parity primary image to C. Images B and C would represent the true quasar brightness; image A would be a highly magnified image

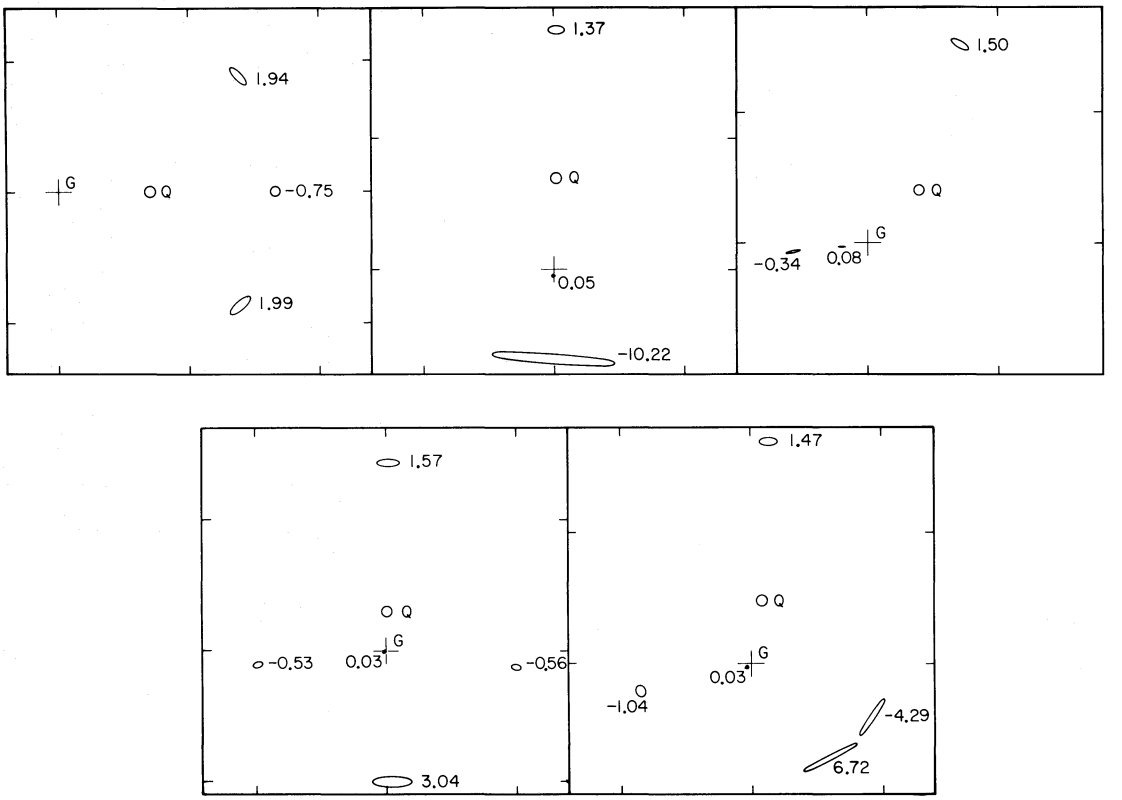

FIG. 7.—Tableau of gravitational lens image solutions using an edge-on massive spiral galaxy. The galaxy, as described in the text, is centered on the cross marked G and has the long axis of the disk-oriented horizontal. A small, circular quasar (Q) is placed as shown to produce images depicted as ellipses of various shapes and sizes (both source and images are drawn greatly enlarged). The magnification is written next to each image and is negative for images of negative parity. Some solutions with three images and some with five are shown; they are typical of the lens solutions for the type of galaxy model used. The lower right solution has two close, bright images near degeneracy. As observed in 1″ seeing, this would resemble the three images Q1115+080A,B,C. There would be an elongation of Q1115+080A due to its being a close double. The tick marks on the axes are at 1″ intervals.

pair about 0".4 apart. This arrangement would explain the apparently enormous intrinsic luminosity of Q1115 +080 (16 mag at $z_s = 1.7$). The CCD pictures show an elongation of the A component in the position angle predicted by the model (see § IV*d*).

The time delays among the images vary from a few months to a year for the models in Figure 7, with the gravitational potential effects being rather more important than the geometrical path length differences. For the model that explains Q1115+080, the time delays are given in Table 8. A large, positive number given in the "delay" column indicates a long wait for the light ray to reach Earth. Thus in this model, image C has the longest delay for brightness variations. The time delays will be increased if other intervening galaxies have a significant bending action on the light beams.

d) *Elongation of Q1115+080A*

If the model we have found in § IV*c* is relevant to Q1115+080, then there is a chance of observing the elongation of image A in the CCD data. We made a special investigation of this possibility. In the delicate comparison of Q1115+080A with a star profile, we had to use star S, which is faint. The main limitation is the accuracy with which the FWHM of S can be determined, but it is the only usable star close to Q1115+080. Visual inspection of the CCD pictures showed Q1115+080A to be clearly elongated in position angle 30° (see Fig. 8); this was not visible in Q1115+080C or any of the stars in the pictures. We decided to use the north-south profile of Q1115+080A in order to quantify this effect.

TABLE 8

TIME DELAYS OF Q1115+080

Image	Magnification	Delay
A1.....	8.72	0.994 yrs
A2.....	−5.29	0.873
B.....	−1.04	0.740
C.....	1.47	1.427
D.....	0.03	0.078

The FWHM was determined by obtaining the north-south profiles of Q1115+080A and of star S and using the interpolation formula (3), adapted for one-dimensional data. The results of these measurements are shown in Table 9 for all the data in which S is sufficiently well exposed to measure its FWHM well. In all but one data frame, we find Q1115+080A to be more elongated north-south than S. The mean size enhancement is 0".088 in the north-south direction over star S.

The model which resembles Q1115+080 in Figure 7 would predict that image A is elongated in position angle 23°, but it does not give a unique separation $\Delta\theta$. If the intensity ratio is ρ, and the north-south separation $\Delta\theta_*$, then

$$\sigma_A^2 = \sigma_S^2 + \Delta\theta_*^2 \rho (1+\rho)^{-2}, \qquad (6)$$

where the Gaussian dispersions of image A and star S

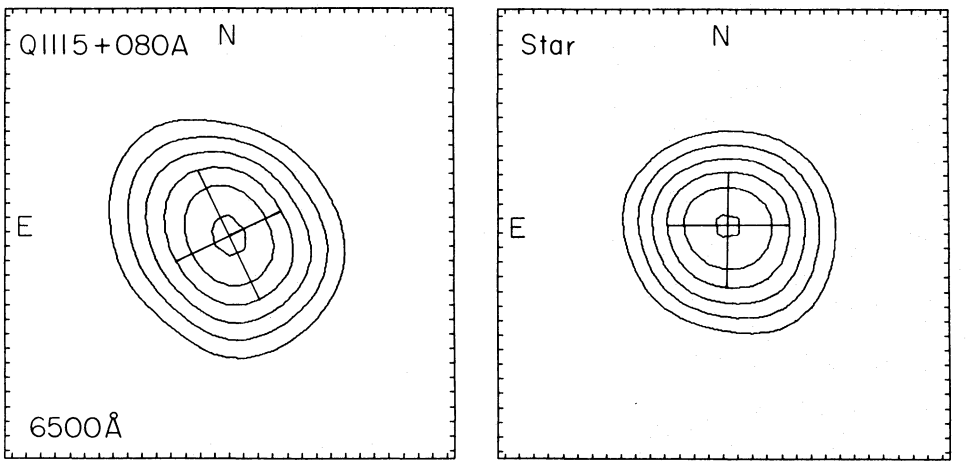

FIG. 8.—Elongation of Q1115+080A. The data have been treated in two ways to allow the elongation of Q1115+080A to be visible (these effects obscure its visibility in Fig. 4): (i) Components B and C have been subtracted, (ii) the pixels have been interpolated to give a grid 5 times finer (there is 0".0844 between pixels; this is the interval between tick marks in this figure). A random field star has also been interpolated and is shown on the right. The contour plots show the core of the profile only from the 30% level up with linear contour intervals. The crosses in the profile mark the orientation of the major axis of the ellipse of the third contour down. The star is very slightly elongated east-west, but Q1115+080A is somewhat more elongated in P.A. 30°. Such an elongation would result if it were a close double with a separation of 0".5, as our model in Fig. 7 suggests it might be. The seeing in this data frame was about 1".1 and was taken in the *r* band.

TABLE 9

NORTH-SOUTH PROFILE OF Q1115+080A[a]

Filter	FWHM of Q1115+080A	FWHM of Star S	Q−S
r	1".263	1".142	0".121
r	1".385	1".218	0".167
i.....	1".349	1".271	0".078
i.....	1".329	1".304	0".025
g	1".320	1".343	−0".023
r	1".707	1".477	0".230
r	1".433	1".380	0".053
r	1".487	1".431	0".056
r	1".407	1".333	0".074
Mean	1".409	1".321	0".088±0".025

[a]From data on June 14, 15, and 16.

may be approximated by multiplying the FWHM by 0.426. Thence we find,

$$\Delta\theta_* \rho^{1/2}(1+\rho)^{-1} = 0''.21, \quad (7)$$

from the measurements shown in Table 9. For $\rho=1$, $\Delta\theta_*=0''.42$; for $\rho=2$, $\Delta\theta_*=0''.45$. The true separation is then $\Delta\theta=\Delta\theta_*/\cos 30°$, or about 0".5. This is about what the model in Figure 7 predicts.

V. SUMMARY

CCD pictures and spectra support the hypothesis that Q1115+080 is gravitationally imaged. We find:

1. Spectra of the faint B and C images have been corrected for scattered light from the bright A image. The C III] λ1909 emission line appears in all spectra at the same strength (possibly slightly weaker in B) and gives redshifts of A, B, and C which are within 100 km s^{-1} of each other, which is well within the measuring error.

2. Direct imaging in the *gri* bands shows all the images to be quite blue. A and C are the same color, while B is slightly redder. Accurate positions and brightness for all three images have been obtained in all three bands.

3. The direct images show no evidence for a lens galaxy at a surface brightness 29 mag arcsec $^{-2}$ between 5" and 8" from Q1115+080. A small group of 20 mag galaxies lies 15" away from Q1115+080.

4. Some theoretical models of gravitational lens effects by a massive spiral galaxy have been computed. The image arrangements do not usually resemble Q1115+080, but a near degenerate quintuple case was found that does. In this, image A is a highly amplified close double. We see such an elongation of Q1115+080A in the CCD data in the position angle predicted by the model (23°).

We thank Ray Weymann for sending us a preprint in time to allow us to observe the Q1115+080 at the end of its season. We thank Don Schneider for running the CCD data system during the observing run, and Walt Morgan and Skip Staples for assistance at the telescope. This research was supported in part by the National Science Foundation grants AST 76-80801, 78-24842, 77-04182, and 80-03398, and by the National Aeronautics and Space Administration through contract NGL05-002-134.

REFERENCES

Gunn, J. E., Hoessel, J. G., and Westphal, J. A. 1981, in preparation.
Thuan, T. X., and Gunn, J. E. 1976, *Pub. A.S.P.*, **88**, 543.
Wade, R. A., Hoessel, J. G., Elias, J. H., and Huchra, J. P. 1979, *Pub. A.S.P.*, **91**, 35.
Weymann, R. J., Latham, D., Angel, J. R. P., Green, R. F., Liebert, J. W., Turnshek, D. A., Turnshek, D. E., and Tyson, J. A. 1980, *Nature*, **285**, 641.
Young, P. J., Gunn, J. E., Kristian, J., Oke, J. B., and Westphal, J. A. 1980, *Ap. J.*, **241**, 507 (Paper I).
_____. 1981, *Ap. J.*, **244**, 736 (Paper II).

JAMES E. GUNN and PETER YOUNG: Robinson Laboratory of Astrophysics, 105-24, California Institute of Technology, Pasadena, CA 91125

JEROME KRISTIAN: Mount Wilson and Las Campanas Observatories, 813 Santa Barbara Street, Pasadena, CA 91101

ROBERT S. DEVERILL and JAMES A. WESTPHAL: Division of Geological and Planetary Science, 170-25, California Institute of Technology, Pasadena, CA 91125

1981ApJ...244..723Y

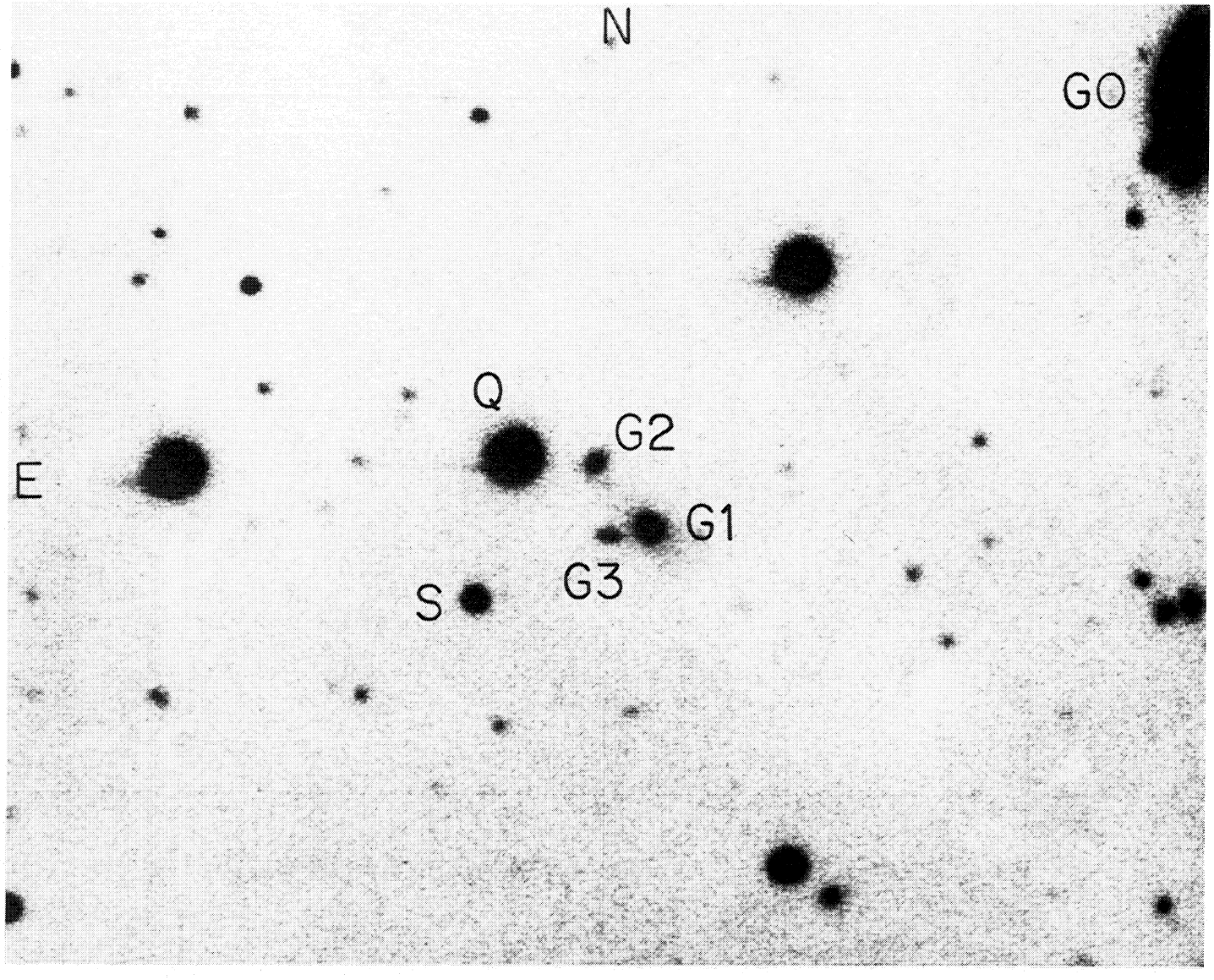

FIG. 6.—CCD picture of the field around Q1115+080 (labeled Q). This is a 2000-second exposure in the *r* band. The field is 3.′16 east-west. The faintest objects visible have an *r* magnitude of 25. North is up and east to the left. Star S and galaxies G0, G1, G2, and G3 are labeled.